A Free and Fast Three-Dimensional/Two-Dimensional Solar Cell Simulator Featuring Conductive Boundary and Quasi-Neutrality Approximations

Andreas Fell

***Abstract*—Details of Quokka, which is a freely available fast 3-D solar cell simulation tool, are presented. Simplifications to the full set of charge carrier transport equations, i.e., quasi-neutrality and conductive boundaries, result in a model that is computationally inexpensive without a loss of generality. Details on the freely available finite volume implementation in MATLAB are given, which shows computation times on the order of seconds to minutes for a full I–V curve sweep on a conventional personal computer. As an application example, the validity of popular analytical models of partial rear contact cells is verified under varying conditions. Consequently, it is observed that significant errors can occur if these analytical models are used to derive local recombination properties from effective lifetime measurements of test structures.**

***Index Terms*—Conductive boundary, modeling, quasi-neutrality, Quokka, simulation, solar cell.**

I. Introduction

On the path to higher efficiencies of solar cells, designs with localized features, e.g., partial rear contact (PRC) or all back contact (ABC) cells, play an increasing role both in research and industry. The increased complexity and degrees of freedom crucially demands multidimensional modeling for both design optimization and detailed characterization. Different analytical models, mainly applicable to PRC geometries, have been published to date [1]–[4]. While they are easy to use, their application is limited to cases where imposed simplifications and assumptions hold. At the other end of the spectrum, powerful commercial software like Sentaurus Device can be used for full 3-D device physics simulation without major simplifications. However, this comes with the drawbacks of availability and complexity in simulation setup and computational time.

For solar cells, in many cases, the well-known general set of semiconductor equations, consisting of one transport equation for minority and majority carriers and Poisson's equation for the electric potential, respectively, can be simplified without a loss of generality. Alamo and Swanson [5], [6] proposed to treat diffusion at the surface as a recombinative boundary condition. This omits the need to solve the equations in the diffused regions and, thus, the space-charge region. Outside the space-charge region, the quasi-neutrality condition, i.e., the equality of excess carrier densities, can be applied [7].

Recently, two notable implementations of simplified 2-D solar cell models have been made available in CoBoGUI [8] and PC2D [9]. Here, the sheet resistance of the diffusions, which are called conductive boundaries, is introduced to correctly account for its influence on lateral potential variations. Despite its usefulness, CoBoGUI still solves for the full set of semiconductor equations and requires a COMSOL license, whereas PC2D is limited by its inflexible meshing and low computational speed. Both are currently restricted to two dimensions.

To overcome these limitations, we present Quokka, which is an easy-to-use 3-D/2-D finite volume implementation in MATLAB, featuring conductive boundaries and the quasi-neutrality condition. The model, which is based on [8], accounts for nonideal recombination currents at the boundaries and recombination losses in the emitter and is enhanced by contact resistance effects. A compiled version will be made available free of any license on pvlighthouse.com.au with the publication of this paper.

As an application example, Quokka is used to validate analytical PRC models. In particular, devices without front surface diffusion and symmetric devices are simulated and compared with analytical results, as these kinds of test structures are often reported to be used for experimental determination of local recombination properties. In this paper, some of the models' underlying assumptions are checked, for which no validation has been published so far.

II. Model

We follow the model of charge carrier transport in a silicon solar cell as presented in [8]. Here, the quasi-Fermi potentials for electrons φ_{Fn} and holes φ_{Fp} and the electric potential φ_{el} are solved for by a set of three coupled differential equations. By using the quasi-neutrality condition, the model can be reduced to the quasi-Fermi potentials and therefore solely solved

Manuscript received September 19, 2012; revised November 26, 2012; accepted November 27, 2012. Date of publication December 19, 2012; date of current version January 18, 2013. The review of this paper was arranged by Editor A. G. Aberle.

The author is with the School of Engineering, College of Engineering and Computer Science, The Australian National University, Canberra ACT 0200, Australia (e-mail: andreas.fell@anu.edu.au).

Color versions of one or more of the figures in this paper are available online at http://ieeexplore.ieee.org.

Digital Object Identifier 10.1109/TED.2012.2231415

0018-9383/$31.00 © 2012 IEEE

by a set of two differential equations. The benefit is improved computational speed and stability when solving numerically.

A detailed summary of the model equations is given in the succeeding sections, using a p-type base material as an example.

A. Bulk (Base) Equations

The continuity equations of the quasi-Fermi potentials are given by

$$\nabla \cdot (\sigma_n \nabla \varphi_{\mathrm{Fn}}) = q(G - R) \tag{1}$$

$$\nabla \cdot (\sigma_p \nabla \varphi_{\mathrm{Fp}}) = -q(G - R). \tag{2}$$

Here, σ denotes the conductivity of each carrier type; q denotes the elementary charge; and G and R denote the generation and recombination rates, respectively. The injection-dependent conductivities are calculated using Klaassen's mobility model [10]. To calculate the carrier densities n and p from the quasi-Fermi potentials, we consider the expressions with the intrinsic carrier density n_i and the thermal voltage V_t. Thus

$$n = n_i \exp\left(\frac{\varphi_{\mathrm{el}} + \varphi_{\mathrm{Fn}}}{V_t}\right) \tag{3}$$

$$p = n_i \exp\left(\frac{-\varphi_{\mathrm{el}} - \varphi_{\mathrm{Fp}}}{V_t}\right). \tag{4}$$

By using the condition of equal excess carrier densities, i.e., $p \approx n + N_A - n_0$, where N_A is the ionized acceptor density, and $n_0 = n_i^2/N_A$ is the equilibrium electron density, an explicit expression for the electron density is derived, i.e.,

$$n = \exp\left(-\frac{\varphi_{\mathrm{Fp}}}{V_t}\right) \times \sqrt{n_i^2 \exp\left(\frac{\varphi_{\mathrm{Fp}} + \varphi_{\mathrm{Fn}}}{V_t}\right) + \frac{(N_A - n_0)^2}{4} \exp\left(\frac{2\varphi_{\mathrm{Fp}}}{V_t}\right)} - \frac{N_A - n_0}{2}. \tag{5}$$

Note that the common definition of the electric potential is used rather than the intrinsic potential presented in [8].

B. Boundary Conditions

1) Symmetry Planes: At the symmetry planes, the component of the gradient of the quasi-Fermi potentials in the direction of the surface normal, which is defined by the normal vector $\vec{n}$, is zero, i.e.,

$$\vec{n} \nabla \varphi_{\mathrm{Fn}/p} = 0. \tag{6}$$

2) Undiffused Surfaces: Recombination at undiffused surfaces is described by either both the ideal and the nonideal dark saturation current densities J_{01} and J_{02} or the surface recombination velocity (SRV) S. Both concepts are equivalent for ideal recombination and low injection condition with the relation $J_{01} = \mathrm{Sqn}_i^2/N_A$. The electron current is equal to the negative recombination current, i.e.,

$$\sigma_n \vec{n} \nabla \varphi_{\mathrm{Fn}} = -J_{01}\left(\frac{np}{n_i^2} - 1\right) - J_{02}\left(\sqrt{\frac{np}{n_i^2}} - 1\right). \tag{7}$$

Different recombination properties, e.g., at the contacts, can be easily accounted for by spatially dependent J_0/S values. We include an electrical contact with the (base) terminal voltage V_{term} at undiffused surfaces by setting the current density through the contact resistivity r_c equal to the total current density at the boundary. Thus

$$\sigma_n \vec{n} \nabla \varphi_{\mathrm{Fn}} + \sigma_p \vec{n} \nabla \varphi_{\mathrm{Fp}} = \frac{V_{\mathrm{term}} - \varphi_{\mathrm{Fp}}}{r_c}. \tag{8}$$

At regions without external contacts, the contact resistance becomes infinite and sets the total current density into the boundary consistently to zero. By this we mean that a diffused back surface field does not have to be included in the simulations, which comes with the benefit of not having to solve an additional 2-D differential equation. However, this approach is not sufficient if the lateral conductivity of the diffusion has a significant effect.

Note that this implementation of the contact resistance, also in case of a diffused surface (10), correctly accounts for current transfer effects into the contacts.

3) Diffused Surfaces: The conduction of carriers in a diffused layer at the surface is accounted for by a 2-D continuity equation of the majority quasi-Fermi potential φ_{Fdiff} with the sheet resistance R_{sheet}, i.e.,

$$\nabla_t \left(\frac{1}{R_{\mathrm{sheet}}} \nabla_t \varphi_{\mathrm{Fdiff}}\right) = -J_{\mathrm{diff}}. \tag{9}$$

For n-type diffusion (emitter), this gives the boundary condition for the bulk electron quasi-Fermi potential as $\varphi_{\mathrm{Fn}} = \varphi_{\mathrm{Fdiff}}$. The source term J_{diff} is equal to the total current density from the base into the emitter less the current density into the contact, i.e.,

$$J_{\mathrm{diff}} = \sigma_n \vec{n} \nabla \varphi_{\mathrm{Fn}} + \sigma_p \vec{n} \nabla \varphi_{\mathrm{Fp}} - \frac{V_{\mathrm{term}} - \varphi_{\mathrm{Fdiff}}}{r_c}. \tag{10}$$

The hole current density into the boundary is equal to the recombination current density less the current density collected within the diffused layer J_L, which gives the boundary condition for the hole quasi-Fermi potential

$$\sigma_p \vec{n} \nabla \varphi_{\mathrm{Fp}} = J_{01}\left(\frac{np}{n_i^2} - 1\right) + J_{02}\left(\sqrt{\frac{np}{n_i^2}} - 1\right) - J_L. \tag{11}$$

For p-type diffusion (back surface field), the expressions are equivalent with altered carrier types and an inverted sign of the recombination current density.

C. Generation and Recombination

In addition to a basic monochromatic generation model and some predefined profiles, no other generation model is included into Quokka. However, it provides the functionality to load a user-defined generation profile and, optionally, a J_L value,

which can be obtained by free tools, e.g., OPAL [11] and EDNA [12].

Injection-dependent Auger recombination is accounted for by the parameterization given in [13]. For p-type silicon, we additionally consider the boron–oxygen Shockley–Read–Hall recombination rate as parameterized in [14].

III. Discretization

For the discretization of the model equations, we use the finite volume method, which is known to be numerically robust and locally conservative, as it essentially balances the currents of each volume element. Thus, it is capable of sufficiently stable and accurate results on relatively coarse meshes and for locally abruptly changing material properties. This is believed to be advantageous for efficient solar cell simulations considering the local nature of contacts and the high gradient of the minority carrier quasi-Fermi potential close to the emitter boundary at maximum power point/short circuit conditions.

We have employed a nonequidistant orthogonal conformal mesh on a cuboidal solution domain. By that, the element sizes can be adapted to the local features of the cell, thus keeping the total number of elements low, whereas the solution variables and equations can be easily handled by matrix variables and differentiating expressions.

In the following, X, Y, and Z denote the element centroids; and dx, dy, and dz denote the element dimensions in each coordinate direction, respectively. x, y, and z are the indices of the conformal mesh/matrix, where the half-offset, e.g., $x+1/2$, denotes the face values between adjacent elements, e.g., elements x and $x+1$. The discretized expressions are given as an example in the (positive) x-direction only.

A. Bulk Equations

The flux, i.e., current I, at the face between adjacent elements is the finite-difference approximation of the current density times the cross-sectional area, i.e.,

$$I_{x+1/2} = dy\, dz\, \sigma_{x+1/2}\, \frac{\varphi_{F_{x+1}} - \varphi_F}{X_{x+1} - X}. \tag{12}$$

The conductivity at the face is derived by the harmonic average, which provides the best numerical conservation of the solution variable [15]. Thus

$$\sigma_{x+1/2} = \frac{dx_{x+1} + dx}{\frac{dx_{x+1}}{\sigma_{x+1}} + \frac{dx}{\sigma}}. \tag{13}$$

The continuity equations of the quasi-Fermi potentials (1) and (2) are then given by the balance of the face currents, i.e.,

$$I_{x+\frac{1}{2}} - I_{x-\frac{1}{2}} + I_{y+\frac{1}{2}} - I_{y-\frac{1}{2}} + I_{z+\frac{1}{2}} - I_{z-\frac{1}{2}} \pm dx\, dy\, dz\, q(G-R) = 0. \tag{14}$$

1) Boundary Conditions: We derive explicit expressions for the values of the quasi-Fermi potentials in the virtual adjacent elements (see Fig. 1), which can be included in the discretized continuity equations (14) of the elements adjacent to the boundary. By that, we omit additional expressions and variables to be solved numerically.

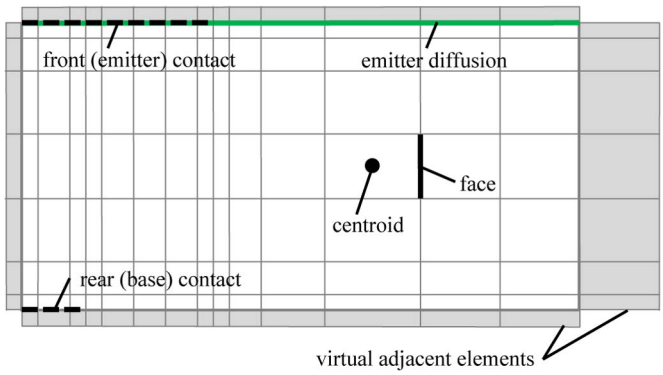

Fig. 1. Exemplary 2-D unit cell solution domain with symmetry planes left and right, front emitter diffusion, and undiffused contacted rear side. Sketch of a conformal orthogonal mesh with refined elements at the contact edges and illustration of mesh terminology.

2) Symmetry Planes: A zero gradient/current density means that the virtual adjacent value is equal to the value in the element next to the boundary, i.e., $\varphi_{Fx+1} = \varphi_F$.

3) Undiffused Surfaces: Equations (7) and (8) give

$$\varphi_{\mathrm{Fn},x+1} = \varphi_{\mathrm{Fn}} - \left[J_{01} \left(\frac{n_{x+\frac{1}{2}} p_{x+\frac{1}{2}}}{n_i^2} - 1 \right) - J_{02} \left(\sqrt{\frac{n_{x+\frac{1}{2}} p_{x+\frac{1}{2}}}{n_i^2}} - 1 \right) \right] \frac{dx}{\sigma_{n,x+\frac{1}{2}}} \tag{15}$$

$$\varphi_{\mathrm{Fp},x+1} = \varphi_{\mathrm{Fp}} + \frac{dx}{\sigma_{p,x+\frac{1}{2}}} \left(\sigma_{n,x+\frac{1}{2}} \frac{\varphi_{\mathrm{Fn},x+1} - \varphi_{\mathrm{Fn}}}{dx} + \frac{V_{\mathrm{term}} - \varphi_{\mathrm{Fp}}}{r_c} \right). \tag{16}$$

4) Diffused Surfaces: Equation (9) is solved in the same way as the bulk continuity equations, reduced by one dimension.

The value for the bulk electron quasi-Fermi potential in the virtual adjacent element is expressed by

$$\varphi_{\mathrm{Fn},x+1} = 2\varphi_{\mathrm{Fdiff}} - \varphi_{\mathrm{Fn}}. \tag{17}$$

Then, the boundary condition for the hole quasi-Fermi potential can be calculated by an expression similar to (15), which is derived from (11).

With the quasi-Fermi potential values at the virtual adjacent elements, the source term J_{diff} can be explicitly calculated by the discretized form of (10), i.e.,

$$J_{\mathrm{diff}} = \sigma_{n,x+\frac{1}{2}} \frac{\varphi_{\mathrm{Fn},x+1} - \varphi_{\mathrm{Fn}}}{dx} + \sigma_{p,x+\frac{1}{2}} \times \frac{\varphi_{\mathrm{Fp},x+1} - \varphi_{\mathrm{Fp}}}{dx} - \frac{V_{\mathrm{term}} - \varphi_{\mathrm{Fdiff}}}{r_c}. \tag{18}$$

Iteration of Boundary Conditions: Note that the discretized expression (15) for the recombination at the boundary is not

explicit, as the unknown carrier densities (and conductivities) at the boundary faces $n/p_{x+1/2}$ are required on the right-hand side. As a first approximation, one could use the centroid values. We rather perform one additional calculation of the boundary conditions by applying (5) to the boundary faces. This iteration greatly improved the convergence and accuracy of the simulations, in particular, when high gradients of the minority carrier quasi-Fermi potential are present and are not finely resolved. Performing more than one iteration showed no further improvement, thus keeping the computational effort lower compared with the accurate treatment of the boundary conditions as additional equations to solve for.

IV. Implementation

The discretized expressions are implemented in MATLAB, making use of its matrix calculation capabilities. By linear indexing, the solution variable matrices are converted into a 1-D vector. We implemented a function to calculate the corresponding vector of the deviations of continuity expressions (14). This nonlinear problem is iteratively minimized by a trust-region-reflective algorithm [16] using the MATLAB built-in function "fsolve." For computational speed, it is crucial to provide the sparsity pattern of the Jacobian matrix. Care was taken with the order of the linear indexing to prevent nonzero elements of the Jacobian matrix far away from the main diagonal.

To keep the total number of elements low and to allow for sweeping of geometry dimensions, a simple fully automated meshing algorithm is implemented in Quokka. It ensures that the minimum mesh size in each coordinate direction is sufficiently low to resolve the smallest feature size with defined accuracy. Beginning at the edges of any features other than the solution domain boundaries, it inflates the mesh sizes in each coordinate direction using an inflation factor, which defines the maximum allowable ratio of adjacent element sizes. This results in a mesh as sketched in Fig. 1.

Quokka features the setting of a defined terminal voltage, iterative open circuit/maximum power point (MPP) finding, and a I–V curve sweep. For the latter, an adaptive sweeping algorithm was implemented to keep the number of simulation points low and thus ensure low computational effort for changing conditions, e.g., within a parameter sweep.

V. Validation

For 1-D cases, Quokka was compared with PC1D with excellent agreement of I–V curves and excess carrier densities in low and high injection. For the validation of the 3-D implementation, we perform a comparison with Sentaurus Device. A PRC unit cell is considered with a 100-μm-wide emitter line contact, two 50 μm $\times$ 150 μm base contacts, and unit cell dimensions of 1000 μm $\times$ 250 μm. We assume a 156-Ω/sq/30-Ω/sq front passivated/contacted selective emitter and derive the J_{01} values for Quokka by EDNA [12] as 15.8 fA/cm^2/272 fA/cm^2. For the bulk, we use a p-type 1.45-$\Omega \cdot$ cm material with an Auger-limited lifetime, and for the rear, a passivated/contacted SRV of 60 cm/s/5000 cm/s. A typical AM 1.5g generation profile is derived by OPAL2 [11], and shading of the front contacts is considered. In X- and Y-direction, we employ a similar mesh, whereas at the front, in z-direction, the mesh in Sentaurus is finer to resolve the diffused region. The I–V curve computation took 30 min in Sentaurus on four CPU cores and 2 min in Quokka on a single CPU core; thus, Quokka proved to be one to two orders of magnitude faster. While almost identical $V_{\rm oc}$ (670 mV) and $J_{\rm sc}$ (37.8 mA/cm^2) was achieved, the fill factor (Sentaurus: 80.0%, Quokka: 80.4%) and efficiency (20.3%, 20.4%) show slight differences. This is attributed to the non-ideal recombination in the emitter and can be corrected for by a J_{02} of 2 nA/cm^2 (maximum difference of I–V curve parameters $< 0.1\%$ rel.). In Fig. 2, the electron density at MPP is compared, evidencing the correct modeling of the bulk carrier transport equations.

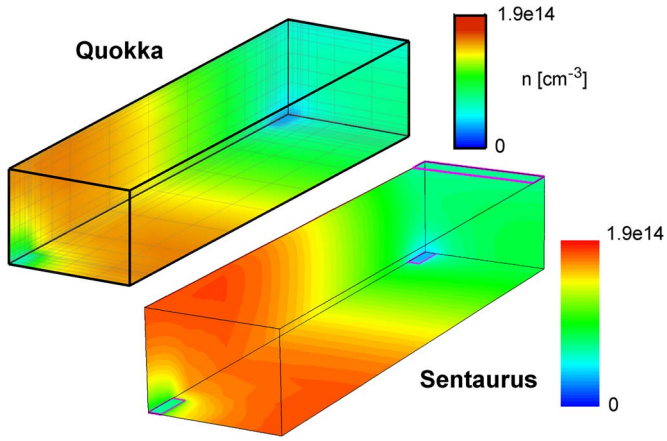

Fig. 2. Quokka–Sentaurus comparison of the electron density n of a PRC unit cell simulation at MPP; contact areas are sketched in the Sentaurus image.

For checking the grid (in)dependence, a 3-D case with relatively large variations in lateral conditions is considered. That is, varying surface recombination parameters and a step function of the generation rate to account for shading of an emitter finger with a width equal to the contact width. Square contact areas are used, as this geometry is accurately adopted by the orthogonal mesh and, thus, does not introduce an additional error by the insufficient resolution of, e.g., circular contacts. I–V curves with varying mesh parameters are calculated, and the accuracy is judged by evaluating the deviation of the fill factor from the solution with a very fine mesh. It was observed that, compared with the other I–V curve parameters ($V_{\rm oc}$, $I_{\rm sc}$, and efficiency) the fill factor deviation is by far the largest and thus represents a lower bound of the simulation accuracy. Additionally, the computation time is shown for calculation of a full I–V curve on an Intel Core i7 processor. Note that the computation time plot is capped at 50 s but actually approaches several minutes for the finest mesh settings.

In Fig. 3 (upper), the results for a high-injection high-series-resistance case with a resulting fill factor of ca. 50% are shown, which is considered to be a worst case scenario for typical solar cell designs. It can be seen that considerably accurate (better than 2%) I–V curves can be achieved with relatively coarse meshes and, consequently, low computation times, in this case, as low as 15 s per I–V curve. In Fig. 3 (lower), a more typical cell design with a fill factor of 79% is shown, showing

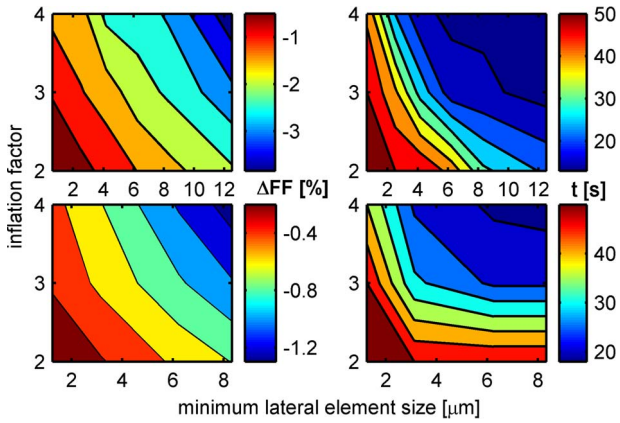

Fig. 3. Relative accuracy of (left) fill factor ΔFF and (right) computation time t dependent on mesh quality for a 3-D PRC unit cell I–V curve simulation; *upper:* worst case scenario with a low fill factor; *lower*: typical case with a good fill factor.

an increased accuracy for the given mesh size and computation time.

VI. Application Example: Validation of Analytical PRC Models

Analytical models for the description of partially contacted solar cells are often used for both cell design optimization and to calculate local recombination properties at the contacts, i.e., S_{cont}. For the latter, the use of symmetrically processed structures [4], [17] or single-side-processed structures without front surface diffusion [18] has been reported. While this is favorable with regard to sample preparation complexity and measurement of effective SRV values, it violates the assumption of a constant excess carrier density at the front surface. To the knowledge of the author, the validation of this simplification has not been published to date.

To check the validity of these simplifications, Quokka simulations are compared with the analytical model presented by Saint-Cast *et al.* [3]. Open circuit conditions, representing contactless lifetime measurements, are used in Quokka, and the effective rear SRV S_{eff} is derived as suggested in [3]. To not influence the simulation results by injection-dependent effects, which are not considered in the analytical model, very low injection conditions (4-mA/cm^2 generation current) are used. A circular contact shape within a square unit cell is considered, which represents the most widely used case. Four different cases are checked as follows: 1) rear contacts with a low front sheet resistance, which is closest to the analytical model; 2) a very high front sheet resistance, representing a case without front diffusion; 3) a symmetric structure with contacts on the front and the rear surfaces placed diagonally to maximize lateral variations; and 4) identical to case 1) but using an accurately simulated series resistance value for the analytical model. Given in the succeeding discussion are the errors of the analytical effective rear SRV error S_{eff}.

From the comparisons in Fig. 4, different sources of errors can be identified. One error comes from the deviation of the front boundary condition when no diffusion is present. This is most obvious for a contact size on the order of the cell thickness, high contact recombination, and contact fractions on

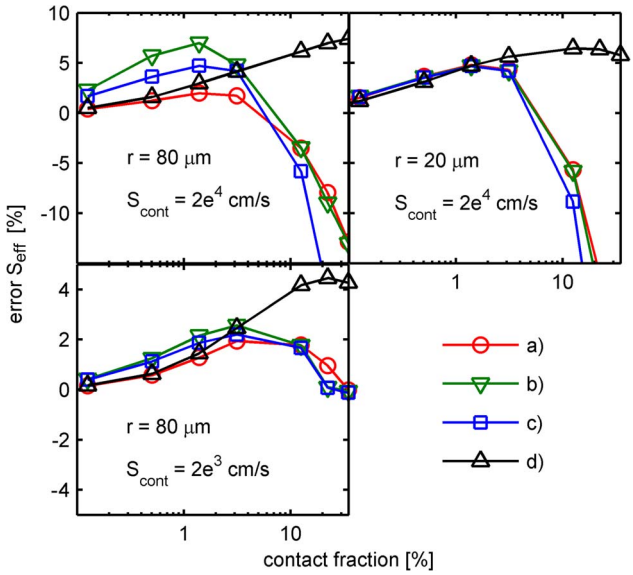

Fig. 4. Error of effective rear SRV with different contact radii r and contact SRV S_{cont}; p-type base resistivity 1.45 $\Omega \cdot$ cm ($N_A = 1\mathrm{e}16 \cdot \mathrm{cm}^{-3}$), bulk lifetime 4.4 ms; S_{pass} 50 cm/s, cell thickness 200 μm, monochromatic illumination at 808 nm, and 0.1 suns equivalent; cases a)–d) are described in the text.

the order of a few percent (see Fig. 4, upper). Interestingly, this error is lower for the symmetric structure compared with a solely rear-processed structure.

A second source of error is the limited accuracy of the analytical expressions used for calculating the series resistance. To account for that, we perform 3-D simulations to accurately determine the series value for each considered geometry and use this value for the analytical model. It can be seen that, for high contact fraction ($> 10\%$) and recombination, this error becomes large in all cases.

Even with an accurate series resistance value, significant errors remain, in particular, for high contact fractions and recombination, which is likely to be related to the nonuniform excess carrier density at the boundaries, as mentioned in [3]. Remarkably, at lower contact recombination, the error is lower for the analytical series resistance expressions (see Fig. 4, lower). This is attributed to the fact that errors with different directions are compensating themselves.

For typical PRC solar cell designs with low contact fractions, the commonly used analytical model produces a reasonably accurate S_{eff} value when S_{pas} and S_{cont} are known. For the reverse operation however, S_{cont} is very sensitive to errors of S_{eff}, in particular, for low contact fractions. For example, a 2% error in S_{eff} at 2% contact fraction results in an error of S_{cont} on the order of 100%. Here, all mentioned errors show a possibly significant contribution. In the simulated cases, only when the contact recombination is below 2000 cm/s and the contact fraction is above 5%, the analytical model gives somewhat reliable S_{cont} values (error $<$ ca. 20%). It is concluded that, when S_{cont} values are derived by model fits, a detailed error analysis, including the aforementioned model inaccuracies, in general, is necessary. Note that additional error sources exist, which are not considered in this paper, in particular, varying front-side optical properties for symmetric structures and laterally varying recombination properties of the contacts.

VII. Conclusion

Quokka, which is the implementation of a simplified solar cell model in MATLAB, has been shown to enable 2-D/3-D unit cell simulations with computational time down to seconds/tens of seconds for a full I–V curve on a conventional personal computer. Compared with the state-of-the-art CoBoGUI model recently presented [8], the more robust finite volume approach, allowing for coarser meshes and solving for two sets of differential equations only, is believed to significantly reduce the computational effort, although this was not tested. Furthermore, Quokka features both 3-D and 2-D and will be made available free of any license on pvlighthouse.com.au.

Limitations of Quokka mainly originate from the conductive boundary simplification: It is not applicable whenever effects at the highly doped surface layers or the space-charge region cannot be approximately accounted for by J_{01}, J_{02}, and J_L values. Quokka also lacks sophisticated optics models but provides an interface to load a generation profile calculated externally.

As an application example, Quokka was used to validate analytical PRC models, i.e., the model presented by Saint-Cast *et al.* [3]. It is found that, while for cell performance calculations the analytical model is reasonably accurate, for the inverse operation, i.e., the derivation of local SRV from, e.g., lifetime measurements, the error can be very high due to error propagation at low area fractions. Different sources of errors were identified to be significant, including inaccuracies of the series resistance expression and violation of the boundary condition assumptions. Thus, these inaccuracies have to be considered in an error analysis of the derived local SRV.

Acknowledgment

The author would like to thank A. Cuevas and K. McIntosh for highly valuable discussions on the modeling, M. Abbott for the efforts of hosting Quokka on pvlighthouse.com.au, and T. Ratcliff for the Sentaurus simulations.

References

[1] B. Fischer, "Loss analysis of crystalline silicon solar cells using photoconductance and quantum efficiency measurements," Ph.D. dissertation, Univ. Konstanz, Konstanz, Germany, 2003.

[2] H. Plagwitz and R. Brendel, "Analytical model for the diode saturation current of point-contacted solar cells," *Progr. Photovolt. Res. Appl.*, vol. 14, no. 1, pp. 1–12, Jan. 2006.

[3] P. Saint-Cast, M. Rüdiger, A. Wolf, M. Hofmann, J. Rentsch, and R. Preu, "Advanced analytical model for the effective recombination velocity of locally contacted surfaces," *J. Appl. Phys.*, vol. 108, no. 1, pp. 013705-1–013705-7, Jul. 2010.

[4] A. Wolf, D. Biro, J. Nekarda, S. Stumpp, A. Kimmerle, S. Mack, and R. Preu, "Comprehensive analytical model for locally contacted rear surface passivated solar cells," *J. Appl. Phys.*, vol. 108, no. 12, pp. 124510-1–124510-13, Dec. 2010.

[5] J. A. del Alamo and R. M. Swanson, "The physics and modeling of heavily doped emitters," *IEEE Trans. Electron Devices*, vol. ED-31, no. 12, pp. 1878–1888, Dec. 1984.

[6] R. M. Swanson, "Point-contact solar cells: Modeling and experiment," *Solar Cells*, vol. 17, no. 1, pp. 85–118, Mar. 1986.

[7] D. A. Kleinman, "The forward characteristic of the PIN diode," *Bell Syst. Tech. J.*, vol. 35, pp. 685–707, May 1956.

[8] R. Brendel, "Modeling solar cells with the dopant-diffused layers treated as conductive boundaries," *Progr. Photovolt., Res. Appl.*, vol. 20, no. 1, pp. 31–43, Jan. 2012.

[9] P. A. Basore and K. Cabanas-Holmen, "PC2D: A circular-reference spreadsheet solar cell device simulator," *IEEE J. Photovolt.*, vol. 1, no. 1, pp. 72–77, Jul. 2011.

[10] D. B. M. Klaassen, "A unified mobility model for device simulation—I. Model equations and concentration dependence," *Solid State Electron.*, vol. 35, no. 7, pp. 953–959, Jul. 1992.

[11] S. C. Baker-Finch and K. R. McIntosh, "A freeware program for precise optical analysis of the front surface of a solar cell," in *Proc. 35th IEEE PVSC*, 2010, pp. 002184–002187.

[12] K. R. McIntosh and P. P. Altermatt, "A freeware 1D emitter model for silicon solar cells," in *Proc. 35th IEEE PVSC*, 2010, pp. 002188–002193.

[13] A. Richter, S. W. Glunz, F. Werner, J. Schmidt, and A. Cuevas, "Improved quantitative description of Auger recombination in crystalline silicon," *Phys. Rev. B, Condens. Matter*, vol. 86, no. 16, pp. 165202-1–165202-14, Oct. 2012.

[14] K. Bothe, R. Sinton, and J. Schmidt, "Fundamental boron–oxygen-related carrier lifetime limit in mono- and multicrystalline silicon," *Progr. Photovolt., Res. Appl.*, vol. 13, no. 4, pp. 287–296, Jun. 2005.

[15] S. V. Patankar, *Numerical Heat Transfer and Fluid Flow*. Washington, DC: Hemisphere Publ. Corp., 1980.

[16] R. H. Byrd, R. B. Schnabel, and G. A. Shultz, "Approximate solution of the trust region problem by minimization over two-dimensional subspaces," *Math. Program.*, vol. 40, no. 3, pp. 247–263, Jan. 1988.

[17] D. Kray and S. Glunz, "Investigation of laser-fired rear-side recombination properties using an analytical model," *Progr. Photovolt., Res. Appl.*, vol. 14, no. 3, pp. 195–201, May 2006.

[18] J. Muller, K. Bothe, S. Gatz, F. Haase, C. Mader, and R. Brendel, "Recombination at laser-processed local base contacts by dynamic infrared lifetime mapping," *J. Appl. Phys.*, vol. 108, no. 12, pp. 124513-1–124513-6, Dec. 2010.

Andreas Fell received the Ph.D. degree in physics from the University of Konstanz, Germany in 2010.

From 2006–2011, he was a researcher at Fraunhofer ISE, Germany. He joined the Australian National University in 2011 as a Research Fellow.